Enhanced Photomultiplication in Filter-Free Organic Photodetectors for R*ed and* NIR Light Sensing Using Minimal Nonfullerene Blends

Linlin Shi[1,4*], *Yaojiang Li*[1], *Jia Jiao*[1], *Ye Zhang*[1], *Guohui Li*[1,2*], *Ting Ji*[1], *Furong Zhu*[3], *Haifeng Lu*[4], *and Yanxia Cui*[1,2*]

[1] College of Electronic Information and Optical Engineering, Key Lab of Interface Science and Engineering in Advanced Materials of Ministry of Education, Key Lab of Advanced Transducers and Intelligent Control System of Ministry of Education, Taiyuan University of Technology, Taiyuan 030024, China
[2]Shanxi-Zheda Institute of Advanced Materials and Chemical Engineering, Taiyuan 030032, China
[3] Department of Physics, Research Centre of Excellence for Organic Electronics, Institute of Advanced Materials, Hong Kong Baptist University, Kowloon Tong, Hong Kong, SAR, China
[4] Yungu (Gu'an) Technology Co., Ltd., Gu'an/Langfang, Hebei 065500, China
*Correspondence author: shilinlinsll@163.com, liguohui@tyut.edu.cn, yanxiacui@tyut.edu.cn

Calculations

The external quantum efficiency and responsivity values of OPDs were derived according to the number of collected charges and the number of incident photons by Equations (1-3):[1]

$$EQE = \frac{J_{ph}/e}{P_{in}/h\nu}, \quad (1)$$

$$EQE = \frac{\chi \tau \mu V}{L^2} \quad (2)$$

$$R = \frac{J_{ph}}{P_{in}} = \frac{EQE \cdot e}{h\nu} \quad (3)$$

J_{ph} is the photogenerated current density (the measured current density under light (J_L) minus the dark current density (J_d)), h is the Planck constant, and ν is the frequency of incident light, $h\nu$ is photon energy, and P_{in} is the illumination power density. χ is the ratio of captured carriers to the total exciton dissociation rate, τ is the lifetime of the captured carriers, V is the value of

the applied bias voltage, μ is the mobility of the uncaptured carriers, and L *is* the device thickness.

D^* of the device calculated from i_n is according to formula (3-4): [2]

$$D^* = \frac{R\sqrt{AB}}{i_n}, \tag{4}$$

A is the active area of the PM-OPDs, B is the bandwidth.

Dynamic range (DR) is referred as the predictable photoresponse generated from the highest and lowest detectable illumination power densities, when the slope (β) of the photocurrent density versus light intensity curve is less than 1, exhibiting the sublinear response. It often exists in the photodetectors with gain or photomultiplication. The photodiodes often show a linear dynamic range (LDR) with β=1. Thus the DR and LDR of the devices are calculated by the following equations: [3-5]

$$DR = 20\log\frac{P_{high}}{P_{low}} \neq 20\log\frac{I_{high}}{I_{low}} \tag{5}$$

$$LDR = 20\log\frac{P_{high}}{P_{low}} = 20\log\frac{I_{high}}{I_{low}} \tag{6}$$

where P_{high} and P_{low} are the highest and lowest detectable illumination power densities of the photocurrent density versus light intensity curve. I_{high} and I_{low} are the highest and lowest photocurrent density of the photocurrent density versus light intensity curve.

Supplementary Figures

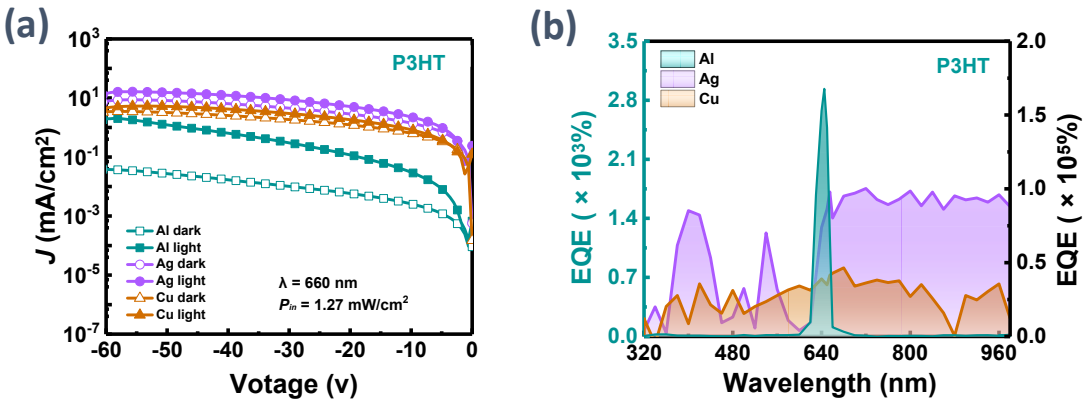

Figure S1 (a) *J–V* characteristics measured for the PM-OPDs with a 2.8 μm thick P3HT active layer in dark and under illumination of the 660 nm LED having a power density of 1.27

mW/cm^2. (b) EQE spectra measured for the P3HT based PM-OPDs with different cathode contacts, operated under the bias of −60 V.

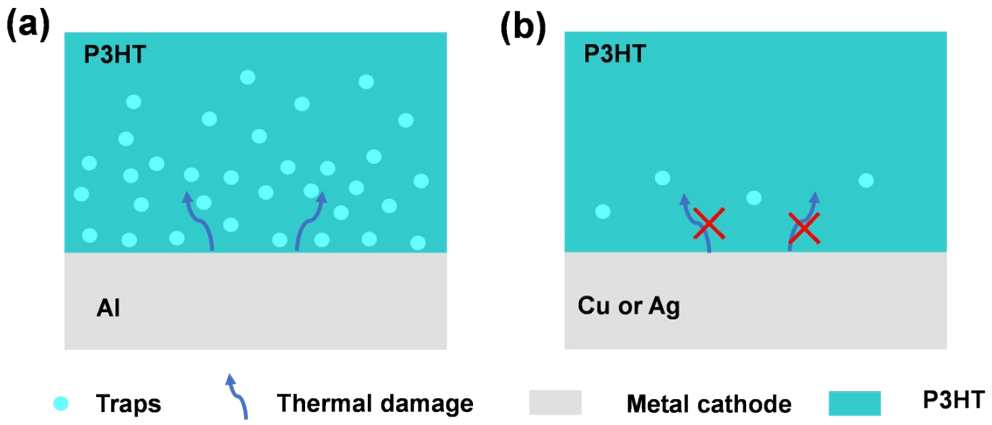

Figure S2 Schematic diagrams illustrating the formation of traps at the (a) P3HT/Al, (b) P3HT/Cu (Ag) interfaces.

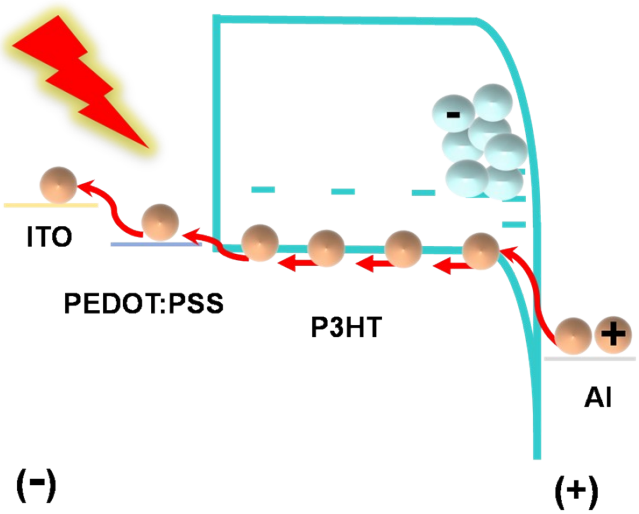

Figure S3 Schematic diagram illustrating the tunneling hole injection at the P3HT/Al interface in a P3HT-based PM-OPD, operated under a reverse bias, under illumination of a 660 nm LED.

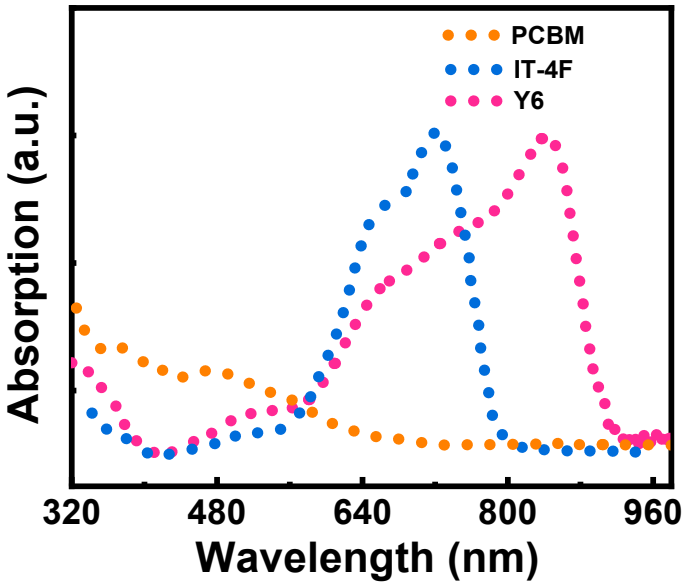

Figure S4 Absorption spectra of the acceptors used in preparation of different PM-OPDs in this work.

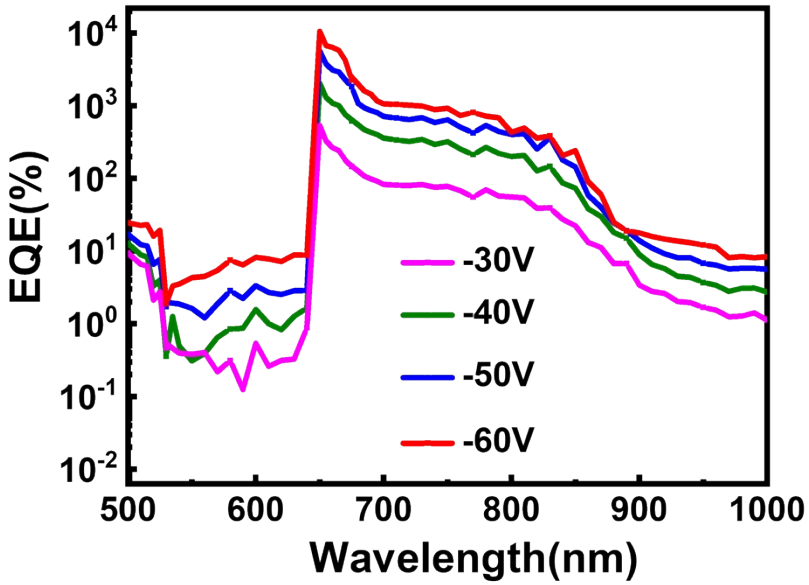

Figure S5 Semi-log EQE spectra of the P3HT:Y6 -based PM-OPD operated at different biases.

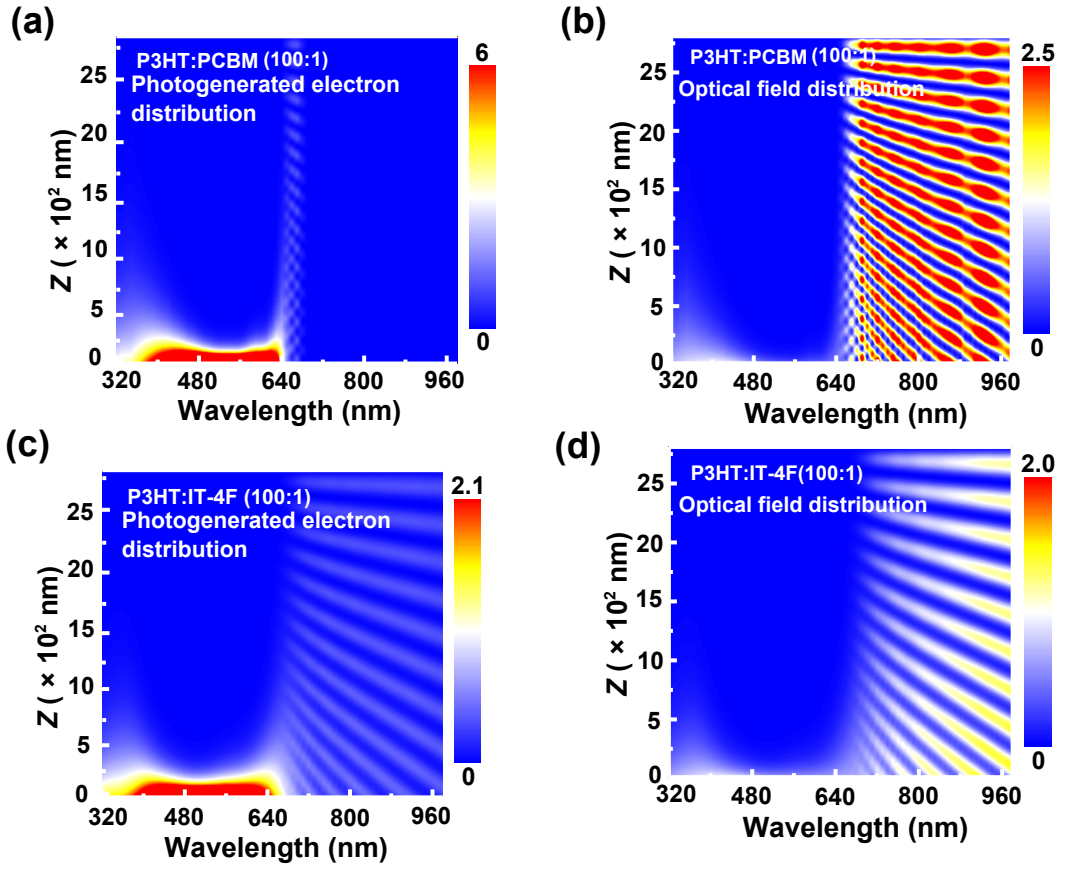

Figure S6 Optical field distribution calculated for PM-OPDs with 2.8 μm thick active layers of (a) P3HT:PCBM (100:1) and (b) P3HT:IT-4F (100:1), and photogenerated electron profiles calculated for PM-OPDs with a 2.8 μm thick active layers of (c) P3HT:PCBM (100:1) and (d) P3HT:IT-4F (100:1).

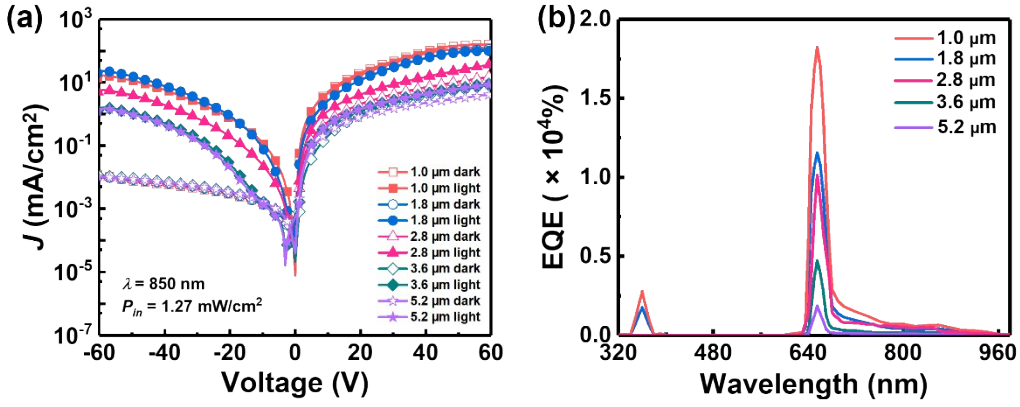

Figure S7 (a) *J-V* characteristic, and (b) EQE spectra operated under the bias of −60 V for P3HT:Y6 BHJ PM-OPD with different active layer thicknesses.

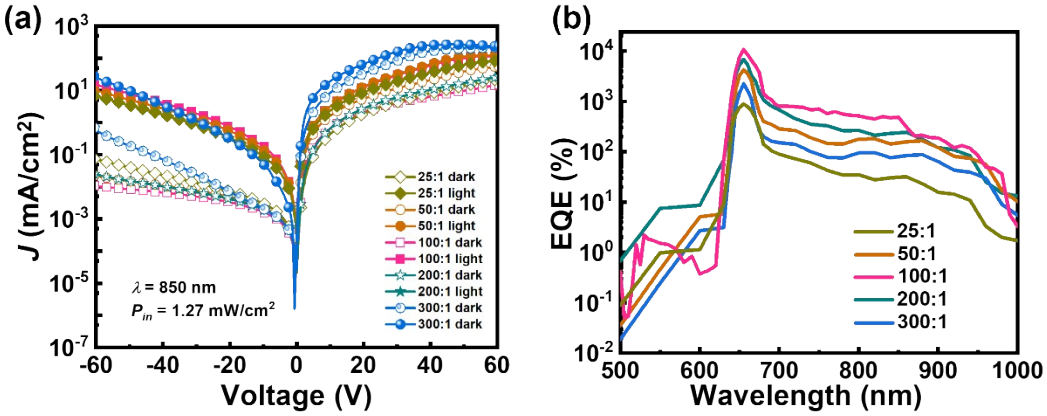

Figure S8 (a) *J-V* characteristic (b) semi-log EQE spectra operated under the bias of −60 V for P3HT:Y6 BHJ PM-OPDs with different D:A ratio.

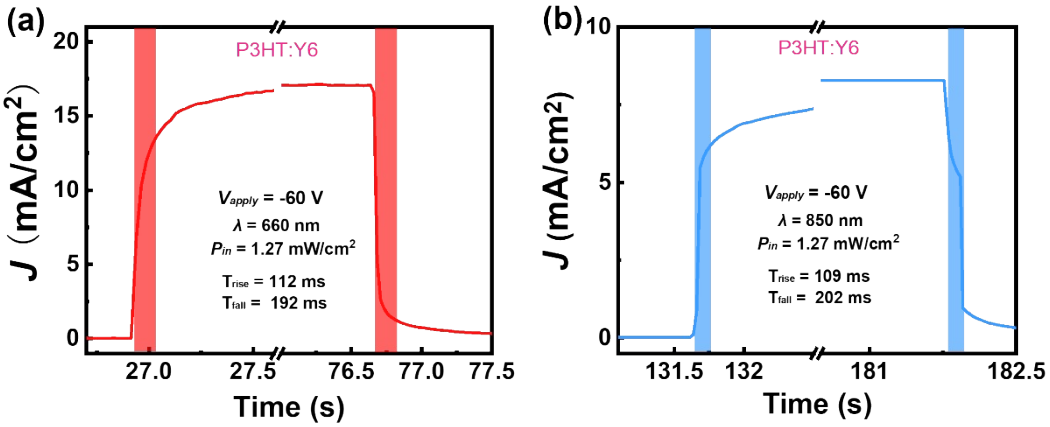

Figure S9 Response times for the P3HT:Y6 BHJ PM-OPD, operated at the bias of −60 V, under illumination of LEDs with emission peak wavelengths of (a) 660 nm and (b) 850 nm.

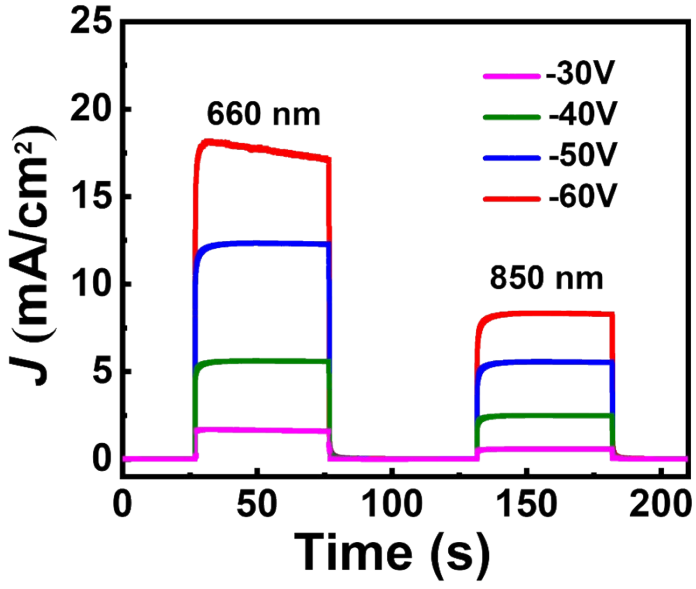

Figure S10 Transient responses measured for the P3HT:Y6 BHJ PM-OPD, operated at different bias, under illumination of LEDs with emission peak wavelengths of 660 nm and 850 nm.

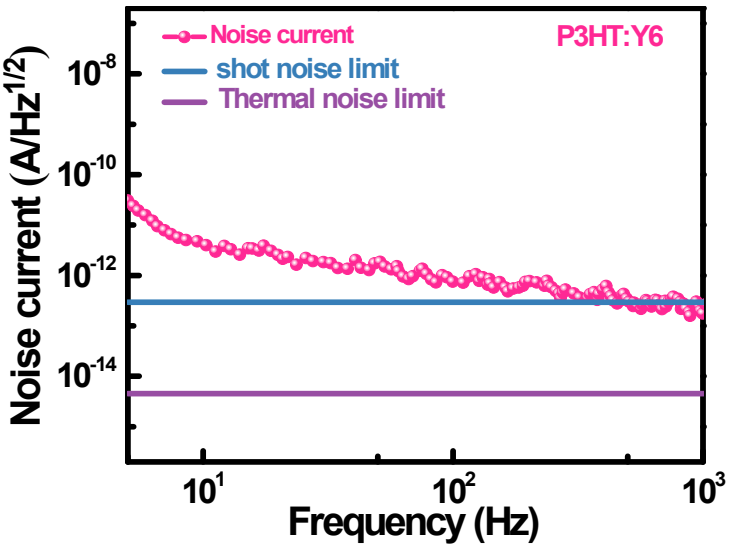

Figure S11 Noise spectral density measured for P3HT:Y6 (100:1)-based PM-OPD operated under bias of −60 V.

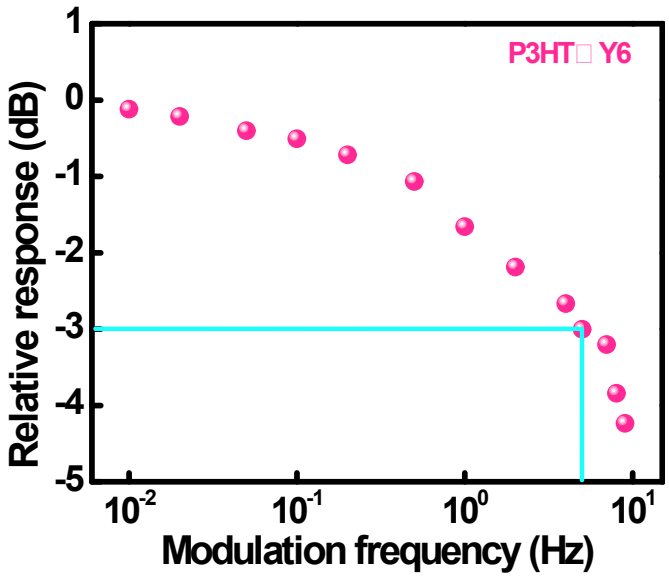

Figure S12 Frequency response of the P3HT:Y6 (100:1)-based PM-OPD operated under bias of −60 V.

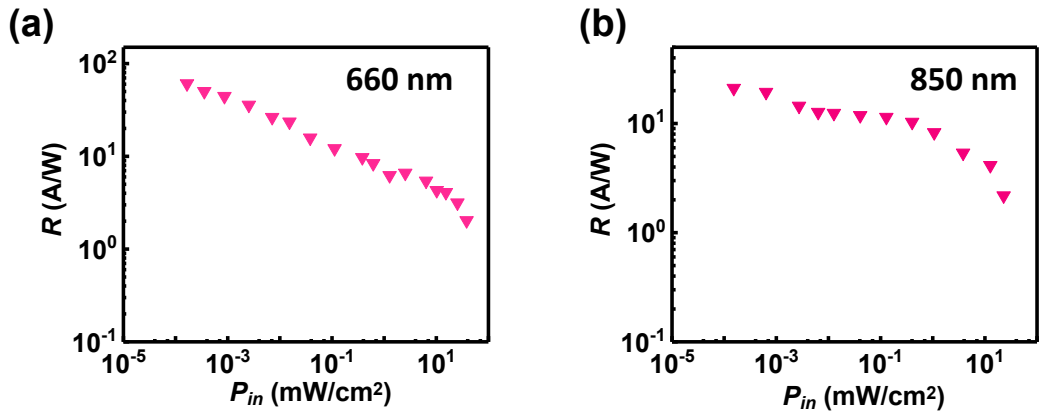

Figure S13 $R(\lambda)$–P_{in} characteristics measured for the P3HT:Y6 (100:1)-based PM-OPD under illumination of (a) 660 nm and (b) 850 nm LEDs.

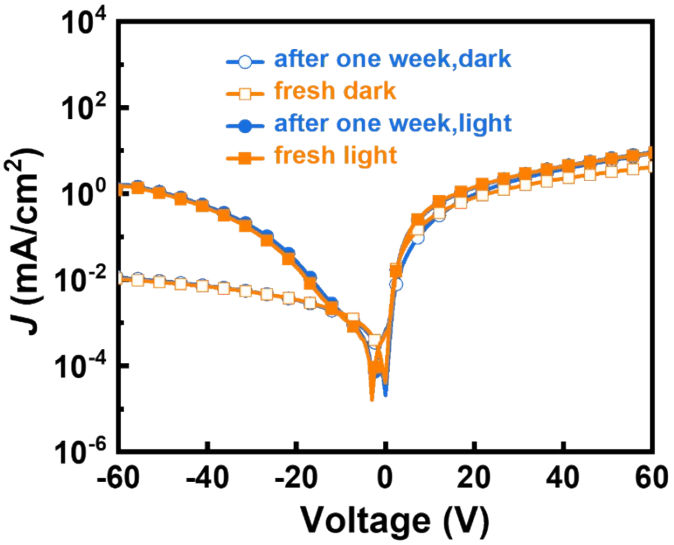

Figure S14 *J*–*V* characteristics in dark and under illumination (850 nm, 1.27 mW/cm^2) of the freshly prepared P3HT:Y6 BHJ PM-OPD device and its corresponding performances after the device aged in air over one week.

References

[1] Shi, L., Chen, K., Zhai, A. et al. Status and outlook of metal–inorganic semiconductor–metal photodetectors. Laser Photonics Rev. 2020; 15: 2000401.

[2] Shi, L., Zhu, Y., Li, G. et al. Atomic-level chemical reaction promoting external quantum efficiency of organic photomultiplication photodetector exceeding 10^8% for weak-light detection. Sci. Bull. 2023; 68: 928-37.

[3] Fang, Y., Armin, A., Meredith, P. & Huang, J. Accurate characterization of next-generation thin-film photodetectors. Nat. Photon. 2018; 13: 1-4.

[4] Wang, Y., Kublitski, J., Xing, S. et al. Narrowband organic photodetectors–towards

miniaturized, spectroscopic sensing. Mater. Horiz. 2022; 9: 220-51.
[5] Pierre, A., Gaikwad, A. & Arias, A. C. Charge-integrating organic heterojunction phototransistors for wide-dynamic-range image sensors. Nat. Photon. 2017; 11: 193-9.